A miniature robot designed for internal inspection of 2-inch ID pipes with elbows

Tao-Yi Wan Department of Mechanical Engineering Department of Mechanical Engineering Department of Mechanical Engineering University of California San Diego La Jolla, USA twan@ucsd.edu

Joonyoung Jang University of California San Diego La Jolla, USA j7jang@ucsd.edu

Thomas R. Bewley University of California San Diego San Diego, USA tbewley@ucsd.edu

Abstract—We present a new spring-loaded miniature robot designed for moving within small pipes, with inner diameters of 2 to 3 inches, including horizontal pipe sections, vertical pipe sections, and elbows. The new robot design comprises two robot arms, two motors, and three omniwheels, using mostly commercial off-the-shelf (COTS) components. The first arm contains a motor and a gear train that drives, in opposite directions, two omniwheels that are pressed against opposite sides of the pipe; these two omniwheels propel the robot down the pipe. The second arm contains a motor and one omniwheel; this omniwheel is used to control the robot's rotation within the pipe. A rod joins the two arms at a rotational joint equipped with a torsion spring, which provides a normal force between the three omniwheels and the inner pipe walls, which generates sufficient traction so that the omniwheels do not slip on the walls. Static analysis reveals the relationship between the spring torque and the normal force between the omniwheels and the walls. Experimental validation of the robot's performance is presented in horizontal pipes, vertical pipes, elbows, and U-shaped pipes. Index Terms-two-inch pipe robot, torsion spring, gear train

I. INTRODUCTION

In the modern world, humans rely on pipelines, which are essential for transporting water, gas, and other vital resources. As a result, inspecting and repairing aging pipelines for defects is crucial. Pipeline leakages and explosions can result in economic losses and threaten human lives, especially in populated areas. However, pipeline inspection is complicated, particularly for those places that are hard to reach, such as underground, the sea floor, high elevations, etc. To address this problem, numerous researchers and engineers have developed different kinds of pipeline robots to assist inspectors in carrying out inspection and repair tasks.

A. Classification of In-pipe Robots

In-pipe robots have different designs to move them through pipelines. We can classify them into eight types based on the in-pipe robot locomotion mechanisms [1] [2]. For example, Fig. 1(a) shows a "PIG" robot, which stands for Pipe Inspection Gauges. This type of robot has two rubber discs on each end of the cylindrical body to accommodate electronic devices. These robots are propelled by the fluid, and fluid pressure difference is generated by rubber discs that block the fluid to drive them passively without an active actuator. However, owing to passive movement, PIGs can only move

in one direction and have poor steerability and control. Zhang et al. [3] found that the robot may damage the inner pipe wall and itself when it attains the maximum speed, known as speed excursion. As shown in Fig. 1(b), a wheeled in-pipe robot has the fastest movement and is the most commercialized type. Their mobility and wheel stability enhance pipeline inspections, maintenance, and navigation while reducing operational failures. Kakogawa et al. [4] described a new multilinkarticulated wheeled robot with four linkages. These robots use omniwheels and hemispherical wheels to fulfill inspections. Fig. 1(c), the caterpillar-type (track) robot comprises the caterpillar mechanism. These robots have larger traction due to the high friction between the pipe and the track wheel. They can drive well on uneven and slippery surfaces. Cui et al. [5] proposed a four-track robot with a differential mechanism that can adapt to various unstructured terrain. A wall-pressing type robot, shown in Fig. 1(d), is supported by arms pressed against the wall for stability. It can adapt to various pipe sizes, providing the necessary force for movement. However, it is complex and bulky. Feng et al. [6] propose a wheeled and wall-pressing type robot for water pipeline cleaning that can be applied to the water pipe for diameters from 1200 to 1500 mm. Fig. 1(e) shows a walking-type robot that moves with legs. It can go through obstacles and has high traction. However, the robot's legs need actuators and motors, which makes the robot bulky and hard to control. Savin et al. [7] considered an in-pipe walking robot with nine links (eight legs and a body) and analyzed the state observer design. Fig. 1(f) shows the inchworm-type robot. It moves forward by repeating the expansion and contraction of its elastic body, but its motion is limited since it can only move one part at a time. Fang et al. [8] proposed an inchworm robot, including a self-locking mechanism, telescopic mechanisms, and a hydraulic system that leverages the robot to have continuous locomotion. Fig. 1(g) shows the screw-type robot. The robot moves forward and backward through rotational motion on a spiral trajectory. Fig. 1(h) shows the snake-type robot that moves in a squirming motion with many actuated joints.

Mills et al. [1] analyzed 1987 to 2015 in-pipe robots. In their review of 234 robots, only 18% of the robots employed a single type, and the wheeled robot has attracted the most attention over the past 30 years. The most common method of generating in-pipe traction was wall-pressing, accounting for 44% of robotics research. The swimming/propeller robot is not mentioned in our classification. However, it was categorized as a type in Mills's papers. This type of robot can move without relying on walls and uses a transported fluid medium to navigate pipelines; However, it cannot move if the medium is not present.

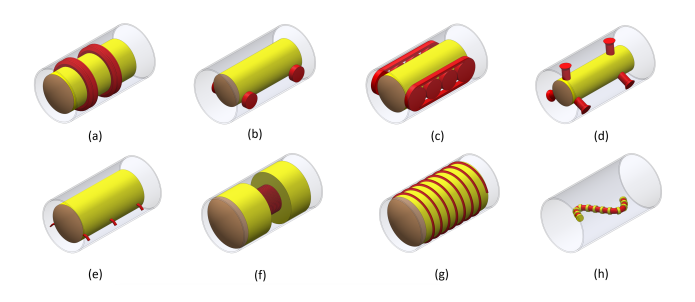


Fig. 1. Locomotion mechanisms types in-pipe robots

B. Robot Mechanism Integration

We aim to build an inspection pipe robot that moves fast in straight pipelines (horizontal and vertical) and elbows. Due to the limited space in pipeline, we require a small, lightweight design with few actuators. Therefore, we design a maneuverable robot with two types of mechanisms (wheeled and wall-pressed), as shown in Fig. 2. With the wheeled mechanism, our robot can move relatively faster than the walking, inchworm, and snake-type mechanisms. With the wall-pressed mechanism, our robot can move in the vertical pipe, as the friction between the inner pipe wall and omniwheel supports the robot to prevent it from falling. The rest of the paper is organized as follows: (II) Miniature robot's mechanical design and control system, (III) Static analysis of the robot in the straight pipes and elbow, (IV) Simulation of the miniature robot, (V) Experiment, and (VI) Conclusion and future work.

II. MINIATURE ROBOT'S MECHANICAL DESIGN AND CONTROL SYSTEM

TABLE I SPECIFICATION OF THE ROBOT

Adaptive pipe inner diameter	2 inch
Total length (when extended)	142 mm
Total weight (without cable)	144 g
Torsion spring (maximum torque)	0.17 N-m
Nominal voltage	DC 6 V
Communication	bluetooth and cable

A. Mechanical design

This miniature robot is built with two robot arms and three 38mm omniwheels; it looks like the letter "V," and most of the components are off-the-shelf. The first arm is mainly for the robot's transfer, comprising a gear train and a micro DC geared motor. The gear train includes six different sizes of

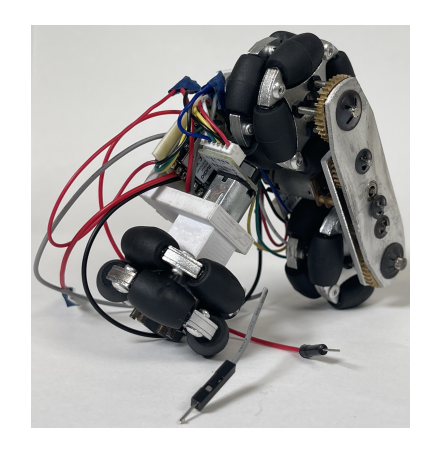


Fig. 2. The miniature robot

brass gears and two aluminum plates that hold the gears. With the gear train, the robot can transfer with only one DC motor, and the two omniwheels can rotate simultaneously (in opposite directions) to drive the robot forward and backward.

The second arm is for the robot's rotation, composed of a 3D-printed arm holding the micro DC motor, and the DC motor connects to an omni-wheel. Each DC motor is connected to the 210:1 gearbox and an encoder.

The two arms are connected by an aluminum rod and a torsion spring, which defines the wall-pressed mechanism mentioned in the introduction. The torsion spring provides enough pressure between the omniwheels and the inner pipe walls to prevent the robot from falling.

B. Control system

The control system of the robot, shown in Fig. 3, contains one microcontroller and one motor controller. The microcontroller is Seeed Studio XIAO nRF52840 Sense, which includes 6 Degree of Freedom (DOF) Inertial Measurement Unit (IMU) and Bluetooth Low Energy (BLE). The 6 DOF IMU contains 3-axis gyroscopes plus a 3-axis accelerometer, which can measure the robot's position and acceleration in three dimensions. The IMU data can be transferred to the computer through the tether, so we can control the robot through a computer or cellphone. Controlling the robot wirelessly at low energy cost is possible using the BLE and a cellphone app.

Since the robot has two 6V DC motors, we chose the motor controller from Pololu "Motoron M2T550 Dual I²C Motor Controller", which can control two DC motors by using an I²C interface. As for the power supply, we use two different voltages for the power system to drive the robot: 3.3V supply for the microcontroller and motor controller and 6V for the two motors.

III. STATIC ANALYSIS OF THE ROBOT

A. Kinematic constraints

The robot contacts the inner pipe surface with three omniwheels (two driving omniwheels and one control omniwheel), and the torsion spring connecting the robot arms provides

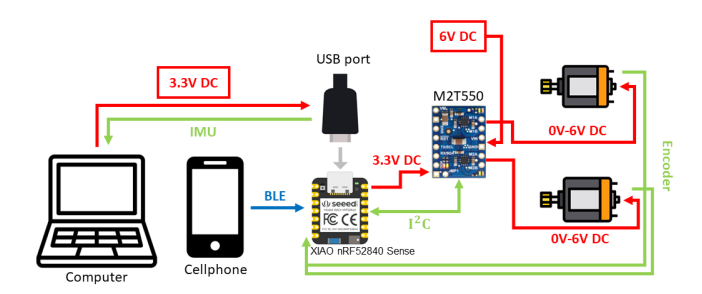


Fig. 3. Control system of the robot

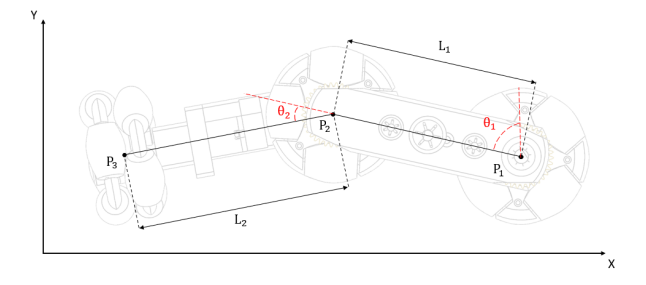


Fig. 4. The angle of the arms in the robot

enough torque to prevent slipping, especially in the vertical pipe where it supports the weight of the robot. The arm with the gear train is called arm1 with length L_1 . The other is called arm2 with length L_2 . The angle between the vertical line and arm1 is called θ_1 , and the angle between the arm1 and arm2 is called θ_2 , as shown in Fig. 4. In the following statements, we analyzed the θ_1 and θ_2 in different conditions.

TABLE II PARAMESTERS OF ROBOT

Arm1 length (L_1) (mm)	54
Arm2 length (L_2) (mm)	60.1
Omni-wheel width (W) (mm)	9.35
Radius of the driving wheel (R) (mm)	19.05
Radius of the control wheel (R_r) (mm)	18.38
Pipe inner diameter (D) (mm)	50.8
Radius of pipeline (R_b) (mm)	50.8

1) Constraints in straight pipe: Observing the robot in the straight pipeline (horizontal and vertical pipeline), we found a small gap (ΔH) between the driving omni-wheel and the inner pipe wall, as shown in Fig. 5. The pipe diameter is D; the vertical distance between two driving wheels is H; the radius of the omni-wheel is R, and the distance between a pair of an omni-wheel is W. From geometrical relations, we calculate the H and ΔH by

$$H = \sqrt{D^2 - W^2}, \quad \Delta H = \frac{1}{2}(D - H).$$

When the robot is moving in the straight pipeline, the angles θ_1 and θ_2 are

$$\theta_1 = \cos^{-1} \frac{D - 2R - 2\Delta H}{L_1},$$
(1)

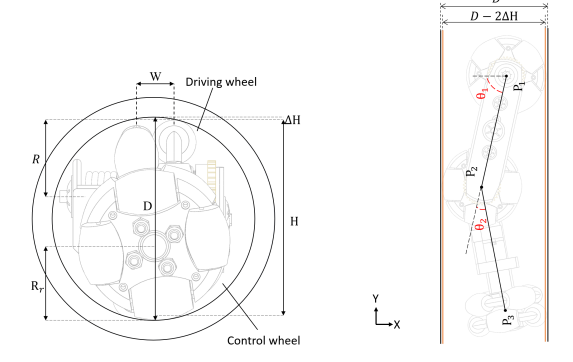


Fig. 5. The miniature robot in straight pipe

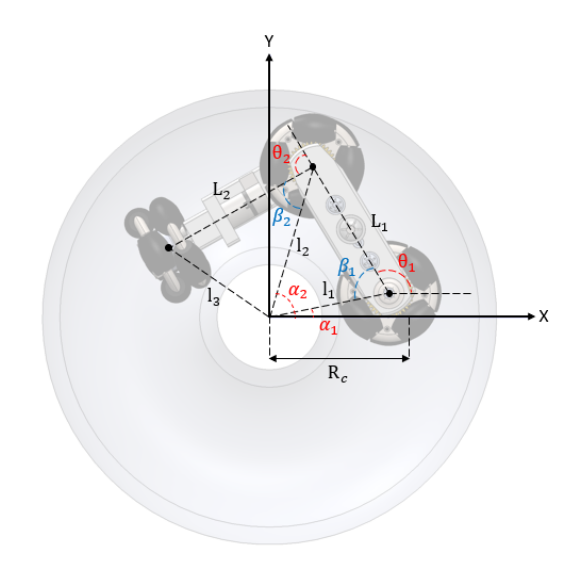


Fig. 6. The miniature robot in the donut (curvilinear motion)

$$\theta_2 = \cos^{-1} \frac{-D + R_r + R + \Delta H}{L_2} - \theta_1.$$
 (2)

From TABLE II, the angles for the robot in the straight pipe are $\theta_1=77.35^\circ$ and $\theta_2=25.07^\circ$.

2) Constraints in donut: We analyze the robot in four different elbow situations with the donut. From Fig. 6, we use cartesian coordinates in the diagram when the robot is in the donut (curvilinear motion), and the θ_1 and θ_2 can be geometrically calculated by

$$\theta_1 = \pi - \beta_1 + \alpha_1,\tag{3}$$

$$\theta_2 = \pi - \beta_2 + \alpha_2 - \theta_1,\tag{4}$$

where α_1 , α_2 , β_1 and β_2 can be calculated by the trigonometric functions

$$\alpha_1 = \tan^{-1} \frac{y_1}{x_1}, \quad \alpha_2 = \tan^{-1} \frac{y_2}{x_2},$$

$$\beta_1 = \cos^{-1} \frac{l_1^2 + L_1^2 - l_2^2}{2l_1 L_1}, \quad \beta_2 = \cos^{-1} \frac{l_2^2 + L_2^2 - l_3^2}{2l_2 L_2}.$$

The α and β angles can be written in the general form

$$\alpha_i = \tan^{-1} \frac{y_i}{x_i}, \quad \beta_i = \cos^{-1} \frac{l_i^2 + L_i^2 - l_{i+1}^2}{2l_i L_i} \ (i = 1, 2).$$

The length l_1 , l_2 and l_3 can be calculated by

$$l_1 = R_c - \frac{D}{2} + R + \Delta H, \quad l_2 = R_c + \frac{D}{2} - R - \Delta H,$$

$$l_3 = R_c - \frac{D}{2} + R_r,$$

where R_c is the radius of the donut's curvature. If the robot moves in the straight pipeline, R_c is infinite, and the formulas θ_1 and θ_2 will be the same as equation (1) and (2).

From TABLE II, the angles for the robot in the elbow are $\theta_1=121.92^\circ$ and $\theta_2=88.41^\circ$.

B. Static analysis of robot

When the robot is inside a pipeline, the omniwheels tightly contact the inner surface of the pipe due to the torsion spring. As the torsion spring creates more torque, the omniwheels gain more friction. However, we managed to avoid too much friction, as it would require more energy to drive the robot. Given the limited space inside the robot, it is important to carefully select the torsion spring. The standard of choosing a torsion spring must fulfill the following requirements. First, the torsion spring provides enough torque to prevent the driving wheel from slipping. Second, the size needs to be suitable for the internal space of the robot. Third, the torsion spring must prevent too much torque when the robot is in the elbow.

1) Static analysis in straight pipe: When the robot moves vertically upward in the pipeline, we need to consider gravity, normal force, rolling friction, and torque generated by the torsion spring deformation, as shown in Fig. 7 where the angle $\phi = \pi - \theta_1 - \theta_2$.

The force equilibrium equation of each direction is

$$\begin{bmatrix} N_u - N_d \\ f_u + f_d \end{bmatrix} = \begin{bmatrix} O \\ G \end{bmatrix}, \tag{5}$$

with

$$N_u = \begin{bmatrix} N_1 & N_{23} \end{bmatrix}^{\mathrm{T}}, \quad N_d = \begin{bmatrix} N_{21} & N_3 \end{bmatrix}^{\mathrm{T}},$$

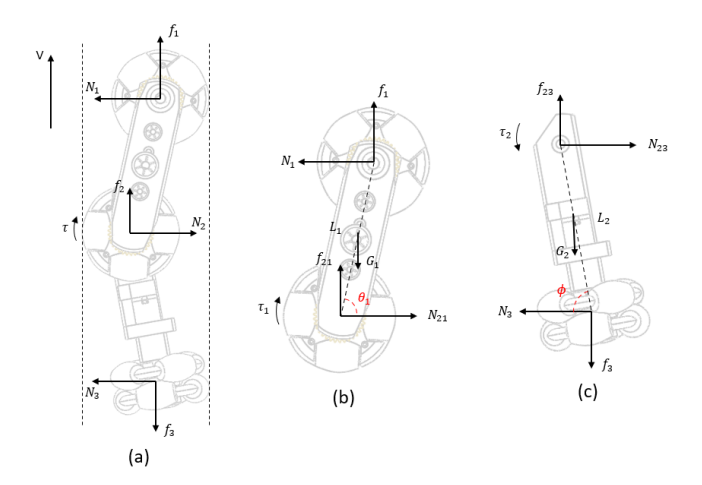


Fig. 7. The robot static analysis in straight pipe

$$G = \begin{bmatrix} G_1 & G_2 \end{bmatrix}^{\mathrm{T}}, f_u = \begin{bmatrix} f_1 & f_{23} \end{bmatrix}^{\mathrm{T}}, f_d = \begin{bmatrix} f_{21} & -f_3 \end{bmatrix}^{\mathrm{T}},$$

where N_1, N_{21}, N_{23}, N_3 are the normal forces of each wheel; f_1, f_{21}, f_{23}, f_3 are the frictions of each wheel while $G_i(i=1,2)$ is the weight of each arm.

With equilibrium of moment for each joint:

$$\tau + \frac{1}{2}\operatorname{diag}(AG)L_c = \operatorname{diag}(N_u)L_s + \operatorname{diag}(Af_u)L_c, \quad (6)$$

where

$$\begin{split} \tau &= \begin{bmatrix} \tau_1 & \tau_2 \end{bmatrix}^{\mathrm{T}}, \quad A = \mathrm{diag}(\begin{bmatrix} 1 & -1 \end{bmatrix}), \\ L_c &= \begin{bmatrix} L_1 \mathrm{cos} \theta_1 & L_2 \mathrm{cos} (\theta_1 + \theta_2) \end{bmatrix}^{\mathrm{T}}, \\ L_s &= \begin{bmatrix} L_1 \mathrm{sin} \theta_1 & L_2 \mathrm{sin} (\theta_1 + \theta_2) \end{bmatrix}^{\mathrm{T}}. \end{split}$$

In the formula, f_3 is the rolling friction which equals $\mu_k N_3$, where μ_k is the coefficient of rolling friction. From the design, we know that the driving force is identical since both of the driving omniwheels connect to the gear train driven by one motor and the gear teeth connect to each omni-wheel are the same, so $f_1 = f_{21} + f_{23} = f_2$.

The driving force should not exceed the maximum static friction to prevent the driving wheels from slipping.

$$f_i \le \mu_s N_i (i = 1, 2),$$
 (7)

where μ_s is the coefficient of maximum static friction.

2) Static analysis in the donut: The analysis of the robot moving in the donut, as shown in Fig. 8, where $\Gamma_1 = \alpha_2 - \alpha_1$ and $\Gamma_2 = \alpha_3 - \alpha_2 - \alpha_1$.

The equilibrium of force and moment are shown as follows:

$$F_u s_{\alpha_1} + F_d s_{\alpha_2} + \text{diag}(AN_u) c_{\alpha_1} - \text{diag}(AN_d) c_{\alpha_2} = 0, (8)$$

$$-F_uc_{\alpha_1}-F_dc_{\alpha_2}+\operatorname{diag}(AN_u)s_{\alpha_1}-\operatorname{diag}(AN_d)s_{\alpha_2}=G,\ (9)$$

$$AF_uL_1 + AF_dL_2 + \operatorname{diag}(AG)(L_1c_{\alpha_1} + \frac{1}{2}L_c) = -\tau,$$
 (10)

where

$$\begin{split} F_u &= \operatorname{diag}(f_u), \ F_d = \operatorname{diag}(f_d), \ A = \operatorname{diag}(\begin{bmatrix} 1 & -1 \end{bmatrix}), \\ c_{\alpha_1} &= \begin{bmatrix} \cos\alpha_1 & \cos\alpha_2 \end{bmatrix}^{\mathsf{T}}, \ s_{\alpha_1} &= \begin{bmatrix} \sin\alpha_1 & \sin\alpha_2 \end{bmatrix}^{\mathsf{T}}, \\ c_{\alpha_2} &= \begin{bmatrix} \cos\alpha_2 & \cos\alpha_3 \end{bmatrix}^{\mathsf{T}}, \ s_{\alpha_2} &= \begin{bmatrix} \sin\alpha_2 & \sin\alpha_3 \end{bmatrix}^{\mathsf{T}}, \\ L_1 &= \begin{bmatrix} \ell_1 & \ell_2 \end{bmatrix}^{\mathsf{T}}, \quad L_2 &= \begin{bmatrix} \ell_2 & \ell_3 \end{bmatrix}^{\mathsf{T}}. \end{split}$$

With the same condition as that in a straight pipe, f_3 is the rolling friction, which equals $\mu_k N_3$, where μ_k is the coefficient of rolling friction. The driving forces are the same: $f_1 = f_{21} + f_{23} = f_2$.

The driving force should not exceed the maximum static friction to prevent the driving wheels from slipping.

$$f_i \le \mu_s N_i (i = 1, 2),$$
 (11)

where μ_s is the coefficient of maximum static friction.

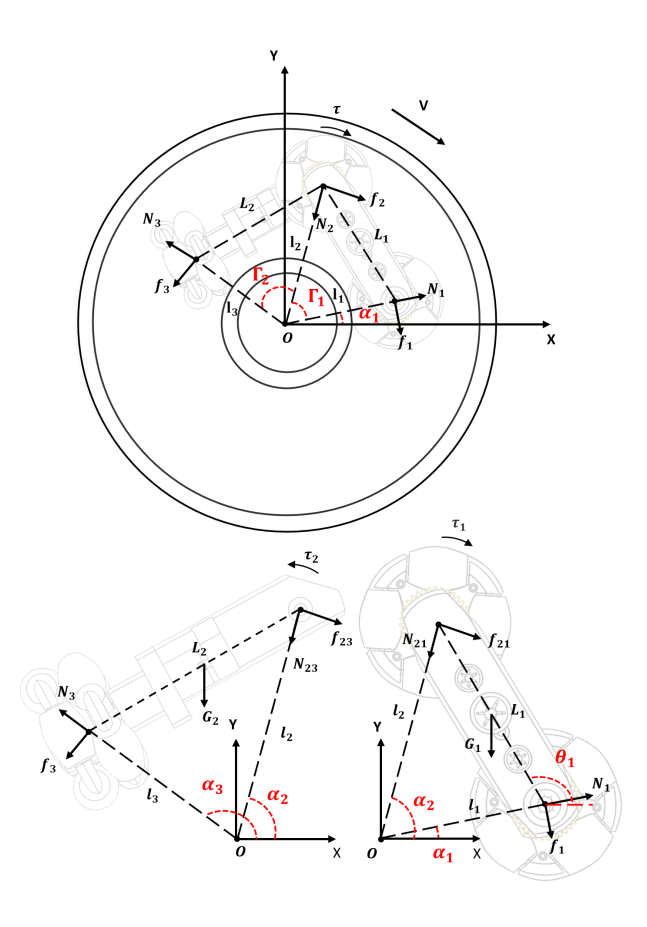


Fig. 8. The robot static analysis in donut

IV. SIMULATION FOR THE MINIATURE ROBOT

The parameters used in the simulation are documented in TABLE II. The static friction coefficient can be estimated by $\tan\alpha~(\alpha$: slope angle). From the simple test, the polyurethane wheels started sliding in the polyvinyl chloride pipe surface at approximately $\alpha=15^{\circ}$, corresponding to $\mu_s=0.27$. Considering the non-uniformity of the pipe's inner surface, $\mu_s=0.25$ was selected for the simulation.

When the robot is in the straight pipeline, from (5)-(7), we can calculate the critical case where the driving force equals the static friction coefficient times the normal force. When the robot is in the critical case, the driving force is 0.52 N, and the torsion spring torque is 108.55 Nmm. Fig. 9 shows that three of the torsion springs are proper when the robot moves in the straight pipe.

When the robot is in curvilinear motion, from (8)-(11), the critical case of the torsion spring torque is less than 80 Nmm. As per our analysis, from (2) and (4), the difference of θ_2 between the straight pipe and the bending pipe is 63.34° . The torsion spring with coefficient k=0.94 Nmm/deg is preloaded at 160° in straight pipe. When the robot is in the bending pipe, the torque decreases to 90.86 Nmm, which is bigger than the critical torque of 80 Nmm. Both of the torsion springs with coefficients k=1.15 (Nmm/deg), and k=1.35 (Nmm/deg)

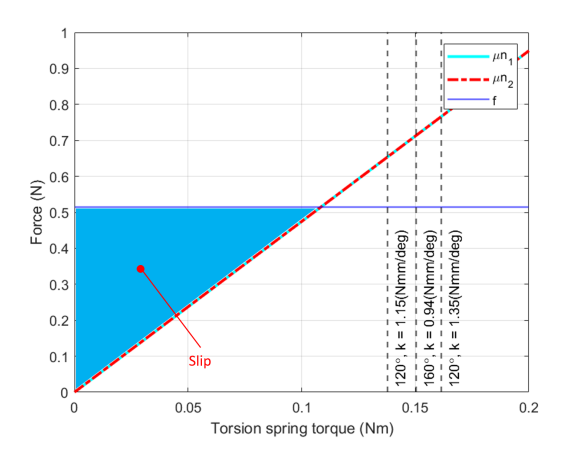


Fig. 9. Selection of torsion spring: required condition to prevent slippage in a vertical straight pipe

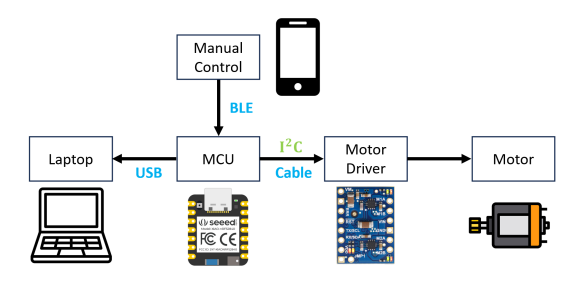


Fig. 10. The control system of the robot

preloaded at 120° in straight pipe have torque less than 80 (Nmm) in the donut. For the experiment, we choose the torsion spring with coefficient k=0.94 Nmm/deg and preload at 160° in straight pipe.

V. EXPERIMENT

The control system of the robot is manually controlled by cellphone through the BLE and open-loop control, as shown in Fig. 10. In the beginning, we tested the robot in a 9.5-inch bend radius pipe, and the robot can pass the pipe smoothly not only when the pipe in the horizontal but in the vertical, as shown in Fig. 11.

To confirm the upper simulation, we tested the robot in the elbow, as shown in Fig. 12 and Fig. 13. The difference between the simulation and the real elbow is that the inner surfaces of the simulation are always connected, whereas, in reality, there is a gap between the elbow and the straight pipe. The robot moves smoothly forward (driving wheel through the elbow); however, there is a risk of the control wheel getting stuck in the gap when it moves backward. In the latter situation, the driving and control wheel must work simultaneously to navigate through the elbow. We also tested the half-donut pipe (U-shaped), as shown in Fig. 14, and the 3-inch 45° elbow. Since the inner wall is continuous, the robot can pass through without any issues.

A video of the experiments is uploaded a https://www.youtube.com/watch?v=T4FRLf7C3kE.

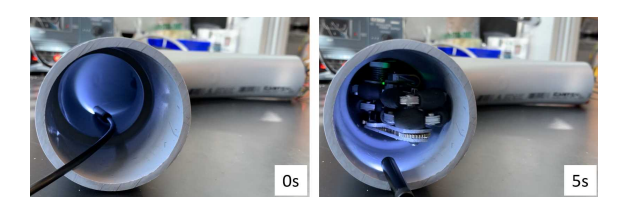


Fig. 11. The robot through the bend radius 9.5-inch pipe

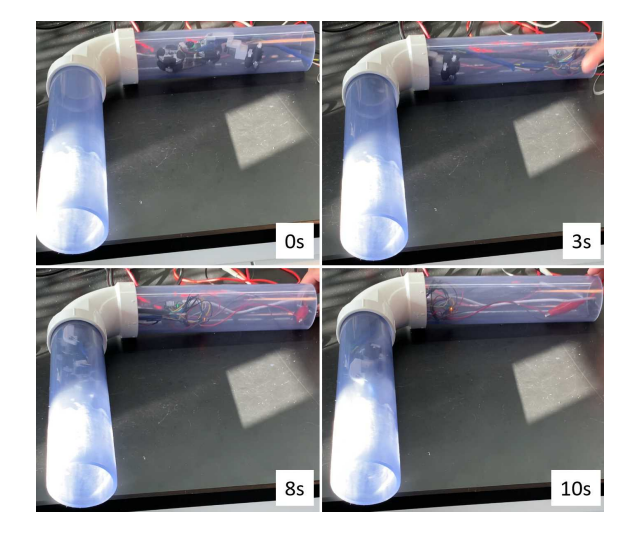


Fig. 12. The robot moves horizontally through the elbow

VI. CONCLUSIONS AND FUTURE WORK

This robot is the most miniature pipe network inspection robot, and it can move freely in 2-inch horizontal pipes, vertical pipes, 9.5-inch bend radius pipes, elbows, half-donut pipes and 3-inch 45° elbow. Simulation results are verified by experiment.

For future work, we will equip the endoscope on the robot for the inspection tasks. Since we designed the robot only moving in 2-inch pipes, the other robot (medium robot for inspection 4 to 6 inches pipeline) will carry the robot within the "capsule," as shown in Fig. 15, to examine 4 to 6 inches pipeline as well as 2-inch pipelines.

ACKNOWLEDGMENT

The authors gratefully acknowledge the financial support of the ERDC Construction Engineering Research Laboratory (CERL) via a subcontract with GTI Energy.

REFERENCES

- G. H. Mills, A. E. Jackson, and R. C. Richardson, "Advances in the inspection of unpiggable pipelines," Robotics 6.4 (2017): 36.
 J. T. Kahnamouei, M. Moallem, "A comprehensive review of in-pipe
- [2] J. T. Kahnamouei, M. Moallem, "A comprehensive review of in-pipe robots," Ocean Engineering 277 (2023): 114260.
- [3] H. Zhang, M. Gao, B. Tang, C.Cui and X. Xu, "Dynamic characteristics of the pipeline inspection gauge under girth weld excitation in submarine pipeline," Petroleum Science 19.2 (2022): 774-788.
- [4] A. Kakogawa and S. Ma. "Design of a multilink-articulated wheeled inspection robot for winding pipelines: AIRo-II," 2016 IEEE/RSJ International Conference on Intelligent Robots and Systems (IROS). IEEE, 2016.

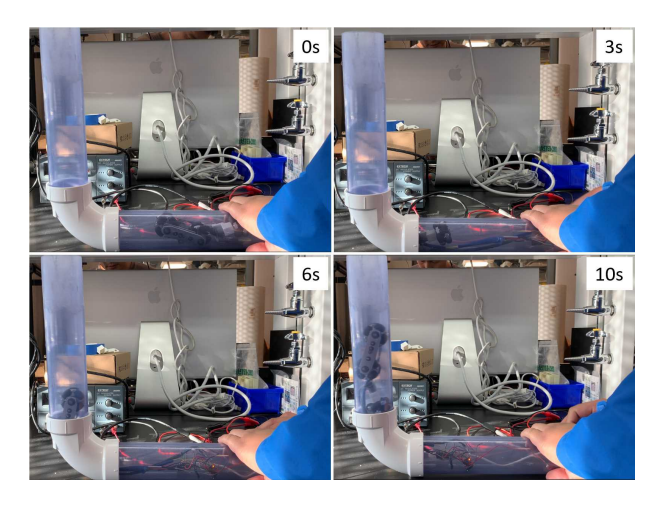


Fig. 13. The robot moves through the elbow from horizontal to vertical directions

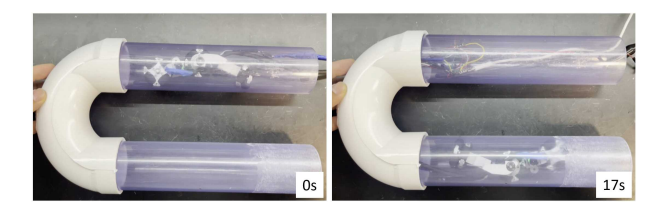


Fig. 14. The robot moves through the U-shaped pipe

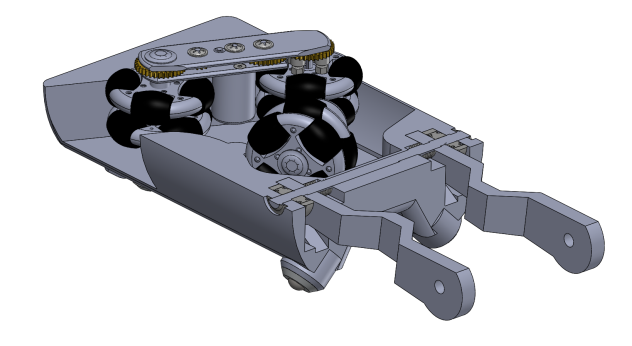


Fig. 15. The capsule for the robot

- [5] J. Cui, Y. Wang, A. Li, S. Shao, and X. Cai, "Design and analysis of tracked robot with differential mechanism." 2018 13th IEEE Conference on Industrial Electronics and Applications (ICIEA). IEEE, 2018.
- [6] G. Feng, W. Li, Z. Li, and Z. He, "Development of a wheeled and wall-pressing type in-pipe robot for water pipelines cleaning and its traveling capability." Mechanics 26.2 (2020): 134-145.
- [7] S. Savin, S. Jatsun, and L. Vorochaeva. "State observer design for a walking in-pipe robot." MATEC web of conferences. Vol. 161. EDP Sciences, 2018.
- [8] D. Fang, J. Shang, Z. Luo, P. Lv, and G. Wu, "Development of a novel self-locking mechanism for continuous propulsion inchworm in-pipe robot." Advances in Mechanical Engineering 10.1 (2018): 1687814017749402.
- [9] T. Li, K. Liu, H. Liu, X. Cui, B. Li, and Y. Wang, "Rapid design of a screw drive in-pipe robot based on parameterized simulation technology." Simulation 95.7 (2019): 659-670.
- [10] Z. Yuan, J. Yuan, and S. Ma, "Design and implementation of a pipeline inspection robot with camera image compensation," the IEEE Int. Conf. Robotics and Automation, pp. 6398-6403, 2020